

Safe Model-based Off-policy Reinforcement Learning for Eco-Driving in Connected and Automated Hybrid Electric Vehicles

Zhaoxuan Zhu, *Student Member, IEEE*, Nicola Pivaro, *Student Member, IEEE*, Shobhit Gupta, *Student Member, IEEE*, Abhishek Gupta, *Member, IEEE* Marcello Canova, *Member, IEEE*

Abstract—Connected and Automated Hybrid Electric Vehicles have the potential to reduce fuel consumption and travel time in real-world driving conditions. The eco-driving problem seeks to design optimal speed and power usage profiles based upon look-ahead information from connectivity and advanced mapping features. Recently, Deep Reinforcement Learning (DRL) has been applied to the eco-driving problem. While the previous studies synthesize simulators and model-free DRL to reduce online computation, this work proposes a Safe Off-policy Model-Based Reinforcement Learning algorithm for the eco-driving problem. The advantages over the existing literature are three-fold. First, the combination of off-policy learning and the use of a physics-based model improves the sample efficiency. Second, the training does not require any extrinsic rewarding mechanism for constraint satisfaction. Third, the feasibility of trajectory is guaranteed by using a safe set approximated by deep generative models.

The performance of the proposed method is benchmarked against a baseline controller representing human drivers, a previously designed model-free DRL strategy, and the wait-and-see optimal solution. In simulation, the proposed algorithm leads to a policy with a higher average speed and a better fuel economy compared to the model-free agent. Compared to the baseline controller, the learned strategy reduces the fuel consumption by more than 21% while keeping the average speed comparable.

Index Terms—Model-based reinforcement learning, generative models, safety-critical applications, connected and automated vehicles.

I. INTRODUCTION

With the advancement in the vehicular connectivity and autonomy, Connected and Automated Vehicles (CAVs) have the potential to operate in a safer and more time- and fuel-efficient manner [1]. With Vehicle-to-Vehicle (V2V) and Vehicle-to-Infrastructure (V2I) communication, the controller has access to real-time look-ahead information including the terrain, infrastructure and surrounding vehicles. Intuitively, with connectivity technologies, controllers can plan a speed profile that allows the ego vehicle to intelligently pass more signalized intersections in green phase with less changes in speed. This problem is formulated as the eco-driving problem,

which aims to minimize weighted sum of the fuel consumption and the travel time between two designated locations by co-optimizing the speed trajectory and the powertrain control strategy [2], [3].

The literature related to eco-driving focuses on different perspectives. Regarding powertrain configuration, the difference is whether the powertrain is equipped with a single power source [3]–[6] or a hybrid electric architecture [7]–[9]. The latter involves modeling multiple power sources and devising optimal control algorithms that can synergistically split the power demand in order to efficiently utilize the electric energy stored in battery. Maamria et al. [10] systematically compares the computational requirements and the optimality of different eco-driving formulations solved offline via Deterministic Dynamic Programming (DDP).

Meanwhile, difference also exists in the complexity of the driving scenarios. Ozatay et al. [4] proposed a framework providing advisory speed profile using online optimization conducted on a cloud-based server without considering the real-time traffic light variability. Olin et al. [9] implemented a eco-driving framework to evaluate real-world fuel economy benefits from in-vehicle testing. As traffic lights are not explicitly considered in these studies, the eco-driving controller is required to be coupled with other decision-making agents, such as human drivers or rule-based controller [11]. Other studies have explicitly modeled and considered Signal Phase and Timings (SPaTs). Jin et al. [3] formulated the problem as a Mixed Integer Linear Programming (MILP) for conventional vehicles with Internal Combustion Engine (ICE). Asadi et al. [12] used traffic simulation models and proposed to solve the problem considering probabilistic SPaT with DDP. Sun et al. [6] formulated the eco-driving problem as a distributionally robust stochastic optimization problem with collected real-world data. Guo et al. [8] proposed a bi-level control framework with a hybrid vehicle.

In this work, the eco-driving problem of Connected and Automated Hybrid Electric Vehicles (CAHEVs) with the capability of passing traffic lights autonomously is studied. With the alternative electrical power source and the V2I communication to receive Signal Phase and Timing messages from signalized intersection, CAHEVs have the potential of significantly reducing the travel time and fuel consumption compared to conventional vehicles. Meanwhile, as the system becomes more complex and autonomous, the control logic becomes more sophisticated and computationally demanding.

Z. Zhu, S. Gupta and M. Canova are with the Center for Automotive Research, The Ohio State University, Columbus, OH 43212 USA (email: zhu.1083@osu.edu; gupta.852@osu.edu; canova.1@osu.edu)

Nicola Pivaro is with Bending Spoons, Italy. The work is done at Center for Automotive Research, The Ohio State University. (email: nicolapivaro@gmail.com)

A. Gupta is with Department of Electrical and Computer Engineering, The Ohio State University, Columbus, OH, 43210 USA (email: gupta.706@osu.edu)

Specifically, the complexities come from three aspects. First, the system dynamics and constraints are nonlinear, non-smooth and non-convex. Second, the driving scenarios are probabilistic. Third, the design of vehicle velocity and battery *SoC* profile requires long-term planning, and a short-sighted policy is subject to local optima.

Recently, the use of Deep Reinforcement Learning (DRL) in the context of eco-driving has caught considerable attention. DRL provides a train-offline, execute-online methodology with which the policy is learned from the historical data or the interaction with simulated environments. Shi et al. [13] modeled the conventional vehicles with ICE as a simplified model and implemented Q-learning to minimize the CO_2 emission at signalized intersections. Li et al. [14] applies an actor-critic algorithm on the ecological ACC problem in car-following mode. Pozzi et al. [15] designed a velocity planner considering the signalized intersection and hybrid powertrain configuration with Deep Deterministic Policy Gradient (DDPG). Zhu et al. [16] formulates the eco-driving problem as a Partially Observable Markov Decision Process (POMDP) and approaches it with Proximal Policy Optimization (PPO). While the strategies with Model-Free Reinforcement Learning (MFRL) in these studies show improvements on the average fuel economy and reductions in onboard computation, the methodology has a fundamental drawback. To teach the agent to drive under complex driving scenarios while satisfying all the constraints from powertrain and traffic rules, a complex and often cumbersome rewarding/penalizing mechanism needs to be designed. Furthermore, under such setup, the agent learns to satisfy constraints by minimizing the expected cost. For scenarios that are rare yet catastrophic, the scale of the cost penalizing constraint violation needs to be significantly larger than the learning objective itself [13]. As a result, such extrinsic rewarding mechanism increases the design period and deteriorates the final performance.

On the other hand, Model Predictive Control (MPC) offers a framework to impose constraints, and the performance can be improved iteratively with a learned terminal cost function (also known as Approximate Dynamic Programming [17]). To be consistent with other works in literature, the technique is referred to as Model-based Reinforcement Learning (MBRL) in this work. Compared to MFRL methods, the advantages are two-fold. First, the method does not require any extrinsic reward to teach agents to satisfy constraints. Instead, the controller satisfies the short-term constraints by formulating an online constrained trajectory optimization problem. Second, the use of model significantly reduces the sample complexity of the learning algorithm [18].

In [19], [20], on-policy MBRL algorithms with known dynamics are proposed for robotic applications. In [21], the system dynamics is learned as ensembles of neural network models, and the online optimization is solved via Cross Entropy Method (CEM). Thananjeyan et.al extended the MBRL algorithm from [21] and the concept of safe set from [22], and proposed the safe on-policy MBRL algorithm for iterative tasks in [23] and multi-start, multi-goal tasks in [24]. In [23], [24], safe sets were approximated by kernel density function, and we extend the idea to a deep generative model for the high-

dimensional safe set approximation. While the use of model increases the sample efficiency in the aforementioned studies, each transition collection becomes more computationally expensive due to the online trajectory optimization. To synthesize the historical data and reduce the overall training wall-time, we propose Safe Model-based Off-policy Reinforcement Learning (SMORL), a safety-critical model-based off-policy Q-learning algorithm for systems with known dynamics. To obtain the value function from Q function, an actor is explicitly trained as in DDPG [25] and Twin Delayed Deep Deterministic policy gradient algorithm (TD3) [26]. As the behavior policy is directly obtained from trajectory optimization and impacted by the learned Q function implicitly, there is a mismatch between the state-action visitation of the target policy and the state-action distribution in the experience buffer collected by the behavior policy. The mismatch, known in offline reinforcement learning [27], causes accumulating bootstrapping error and deteriorates the performance. In this work, Batch Constrained Q-learning (BCQ) [28] is used to address the distributional mismatch.

The contributions of the work are two-fold. First, an off-policy MBRL algorithm SMORL is proposed. The off-policy nature of the algorithm allows the use of experience replay [29] and increases the sample efficiency compared to other MBRL algorithm in literature. Second, the proposed algorithm is successfully applied to the eco-driving problem. Without any extrinsic reward design, the agent trained with SMORL shows dominating performance compared to the one previously trained with MFRL algorithm in [16].

The remainder of the paper is organized as follows. Sec. II presents the simulation environment and the eco-driving problem formulation. Sec. III introduces the preliminaries of the mathematical concepts, and Sec. IV presents the main algorithm SMORL. Sec. V explains the detailed implementation of SMORL on the eco-driving problem. Sec. VI shows the training details and benchmarks the performance. Finally, Sec. VII concludes the study and identifies the future research directions.

II. ECO-DRIVING FOR CAHEVS

A. Environment

As collecting data in the real-world driving data is expensive and potentially unsafe, a model of the environment is developed for training and validation purposes. The environment model, named EcoSim, consists of a Vehicle Dynamics and Powertrain (VD&PT) model and a microscopic traffic simulator. Fig.1 shows EcoSim and its interaction with the controller and the learning algorithm. The controller commands three control inputs, namely, the Internal Combustion Engine (ICE) torque, the electric motor torque and the mechanical brake torque. The component-level torques collectively determine the HEV powertrain dynamics, the longitudinal dynamics of the ego vehicle and its progress along the trip. As in [30], it is assumed that cellular communication technologies are available onboard, and the real-time SPaT information of traffic lights in the geographic region of interest remains available during the trip. The DRL agent utilizes the SPaT

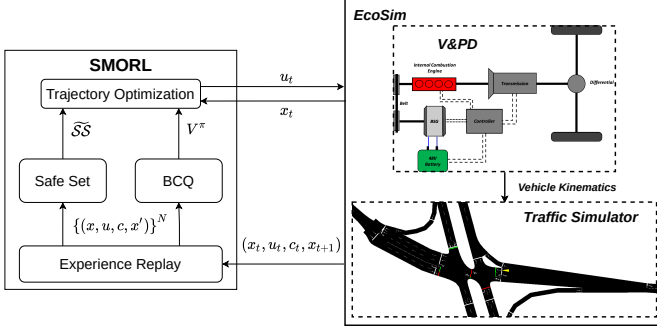


Fig. 1. The Structure of The Environment Model

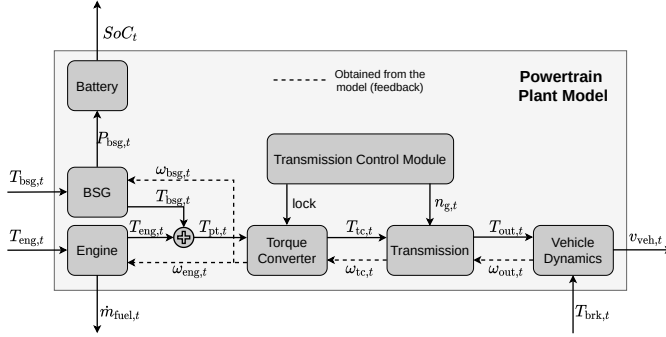


Fig. 2. Block Diagram of 48V P0 Mild-Hybrid Drivetrain.

from the upcoming traffic light while ignoring the SPaT from any other traffic light regardless of the availability. Specifically, the controller receives the distance to the upcoming traffic light, its current status and its SPaT program as part of the observation. Finally, a navigation application with Global Positioning System (GPS) is assumed to be available on the vehicle such that the locations of the origin and destination, the remaining distance and the speed limits along the entire trip are available at every point during the trip.

1) *Vehicle and Powertrain Model*: A forward-looking dynamic powertrain model is developed for fuel economy evaluation and control strategy verification over real-world routes. In this work, a P0 mild-hybrid electric vehicle (mHEV) is considered, equipped with a 48V Belted Starter Generator (BSG) performing torque assist, regenerative braking and start-stop functions. The input/output relation among the modeled powertrain components is illustrated in Fig. 2.

The engine is modeled as low-frequency quasi-static nonlinear maps based on steady state engine test bench data provided by supplier. The map of instantaneous fuel consumption \dot{m}_{fuel} is a function of engine angular velocity ω_{eng} and engine torque T_{eng} , and the maps of torque limits T_{eng}^{\min} and T_{eng}^{\max} are functions of engine angular velocity ω_{eng} .

The battery SoC and voltage V_{batt} are governed by a zero-th order equivalent circuit model shown as follows:

$$I_t = \frac{V_{OC}(SoC_t) - \sqrt{V_{OC}^2(SoC_t) - 4R_0(SoC_t)P_{\text{bsg},t}}}{2R_0(SoC_t)}, \quad (1)$$

$$SoC_{t+1} = SoC_t - \frac{\Delta t}{C_{\text{nom}}}(I_t + I_{\text{aux}}), \quad (2)$$

where t is the discretized time index, and Δt is the time discretization that is set to be 1s in the study. The power consumed by auxiliaries is modeled by a calibrated constant current bias I_{aux} . The cell open circuit voltage V_{OC} and internal resistance R_0 are maps of SoC from a battery pack supplier.

The vehicle dynamics model is based on the road-load equation:

$$v_{\text{veh},t+1} = v_{\text{veh},t} + \Delta t \left(\frac{T_{\text{out},t} - T_{\text{brk},t}}{MR_w} - \frac{C_d \rho_a \Omega_f v_{\text{veh},t}^2}{2M} - g \cos \alpha C_r v_{\text{veh},t} - g \sin \alpha \right) \quad (3)$$

Here, the four terms inside the bracket of the left hand side are associated with the forward propulsion force, the tire rolling resistance, the aerodynamic drag, and the road grade, respectively. T_{brk} is the brake torque applied on wheel, C_d is the aerodynamic drag coefficient, ρ_a is the air density, A_f is the effective aerodynamic frontal area, C_r is rolling resistance coefficient, and α is the road grade.

Besides the aforementioned models, which are directly associated with either the states or the objective in the eco-driving Optimal Control Problem (OCP) formulation, BSG, torque converter and transmission are also modeled in the study. The BSG is modeled as a quasi-static efficiency map to compute the electrical power output P_{bsg} . A torque converter model is developed with the purpose of computing the losses during the traction and regeneration modes. The transmission model is based on a static gearbox, and its efficiency η_{trans} is scheduled as a nonlinear map of the gear number n_g , the transmission input shaft torque T_{trans} and the transmission input speed ω_{trans} . The detailed mathematical models of these components can be found in [16].

The forward vehicle model as shown in Fig. 2 was calibrated and validated using experimental data from chassis dynamometer. Vehicle velocity, battery SoC , gear number, engine speed and the fuel consumption were used to evaluate the model with the experimental data. Fig. 3 shows the sample results from model verification over the FTP-75 regulatory drive cycle. Results indicate that the the vehicle velocity and SoC are accurately predicted by the model. Some of the mismatches in the battery SoC can be attributed to the assumptions made in the simplified battery model such as modeling electrical auxiliary loads as constant current bias. Further, the final value of the fuel consumption estimated by the model over the FTP-75 drive cycle is within 4% of the actual fuel consumption which verifies that the model can be used for energy and fuel prediction over real-world routes.

2) *Traffic Model*: A large-scale microscopic traffic simulator is developed in an open source software Simulation of Urban Mobility (SUMO) [31] as part of the environment. In order to recreate realistic mixed urban and highway trips for training, the map of the city of Columbus, OH, US is downloaded from the online database OpenStreetMap [32]. The map contains the length, shape, type and speed limit of the road segments and the detailed program of each traffic light at signalized intersections. Fig. 4 highlights the area

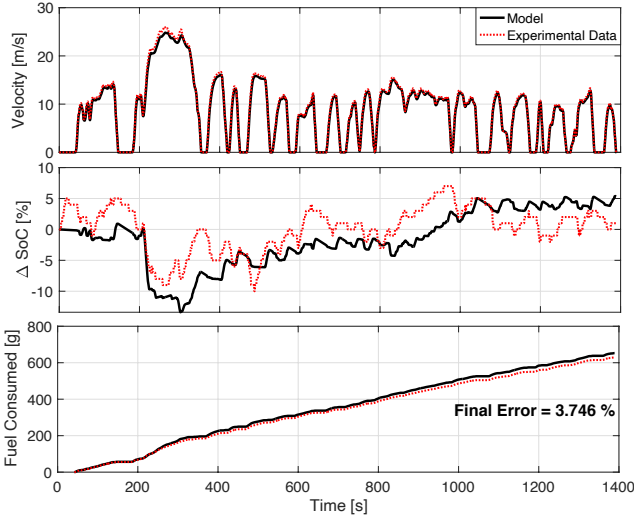


Fig. 3. Validation of Vehicle Velocity, SoC and Fuel Consumed over FTP Cycle.

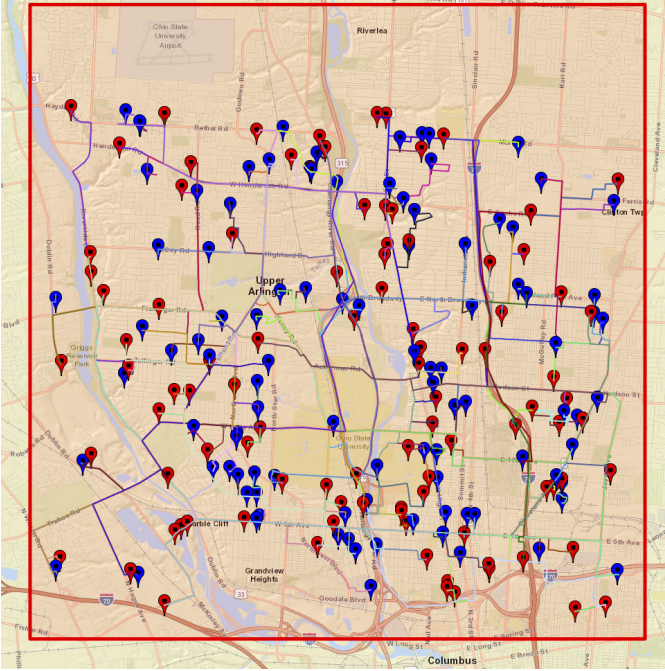


Fig. 4. Map of Columbus, OH as the Traffic Environment for Training

that is covered in the study. In the shaded area, 10,000 random passenger car trips, each of which the total distance is randomly distributed from 5 km to 10 km, are generated as the training set. Another 100 trips, indicated by the origins (red markers) and destinations (blue markers) in Fig. 4, are generated following the same distribution as the testing set. In addition, the departure time of each trip follows a geometric distribution with the success rate $p = 0.01$. The variation and the randomness of the trips used for training enhance the richness of the environment, which subsequently leads to a learned policy that is less subject to local minimum and agnostic to specific driving condition (better generalizability) [33].

The interface between the traffic simulator and the VD&PT model is established via Traffic Control Interface (TraCI) as part of the SUMO package. At any given time, the vehicle speed is calculated based on VD&PT model in response to the component-level torque commands. Subsequently, the location of the ego vehicle and the connectivity information, including SPaT and GPS signals, are determined and updated via TraCI.

B. Optimization Formulation

In the eco-driving problem, the objective is to minimize the weighted sum of fuel consumption and travel time between two designated locations. The optimal control problem is mathematically formulated as follows:

$$\min_{\{u_t\}_{t=1}^{\infty}} \mathbb{E} \left[\sum_{t=1}^{\infty} [\lambda \dot{m}_{\text{fuel},t} + (1 - \lambda)] \Delta t \cdot \mathbb{I}[s_t < s_{\text{total}}] \right] \quad (4a)$$

$$\text{where } u_t = [T_{\text{eng},t}, T_{\text{bsg},t}, T_{\text{brk},t}]^T \quad (4b)$$

$$\text{s.t. } SoC_{t+1} = f_{\text{batt}}(v_{\text{veh},t}, SoC_t, u_t) \quad (4c)$$

$$v_{\text{veh},t+1} = f_{\text{veh}}(v_{\text{veh},t}, SoC_t, u_t) \quad (4d)$$

$$T_{\text{eng}}^{\min}(\omega_{\text{eng},t}) \leq T_{\text{eng},t} \leq T_{\text{eng}}^{\max}(\omega_{\text{eng},t}) \quad (4e)$$

$$T_{\text{bsg}}^{\min}(\omega_{\text{bsg},t}) \leq T_{\text{bsg},t} \leq T_{\text{bsg}}^{\max}(\omega_{\text{bsg},t}) \quad (4f)$$

$$I^{\min} \leq I_t \leq I^{\max} \quad (4g)$$

$$SoC^{\min} \leq SoC_t \leq SoC^{\max} \quad (4h)$$

$$SoC_T \geq SoC^T \quad (4i)$$

$$0 \leq v_{\text{veh},t} \leq v_{\text{lim},t} \quad (4j)$$

$$(t, s_t) \notin \mathcal{S}_{\text{red}}. \quad (4k)$$

Here, $\dot{m}_{\text{fuel},t}$ is the instantaneous fuel consumption. λ is a normalized weight on the fuel consumption. ω_{eng} and ω_{bsg} are the engine and BSG angular velocities, respectively, and they are static functions of vehicle speed v_{veh} and gear number n_g . f_{batt} and f_{veh} are the battery and vehicle dynamics, respectively, introduced in Sec. II-A1. Eqn. (4e) to (4g) are the constraints imposed by the powertrain components. Eqn. (4h) and Eqn. (4i) are the constraints on the instantaneous battery SoC and terminal SoC for charge sustaining, respectively. Here, the subscript T represents the time at which the vehicle reaches the destination. SoC^{\min} , SoC^{\max} and SoC^T are commonly set to 30%, 80% and 50%. Eqn. (4j) and (4k) are the constraints imposed by traffic conditions. The set \mathcal{S}_{red} represents the set in which the traffic light at the certain location is in red phase, as indicated by the red lines in Fig. 5. The problem is formulated as a infinite horizon problem in which the stage cost becomes zero once the system reaches the goal set, i.e. the travelled distance s_t is greater than or equal to the total distance of the trip s_{total} while keeping the terminal SoC_T greater than or equal to SoC^T . In addition, anytime that the vehicle violates the traffic light constraints, i.e. Eqn. (4k), the trip is considered failure and the goal set is not reached.

To solve the aforementioned optimization formulation as an OCP, a MBRL algorithm is proposed, and the preliminaries of the algorithm are included in the next section.

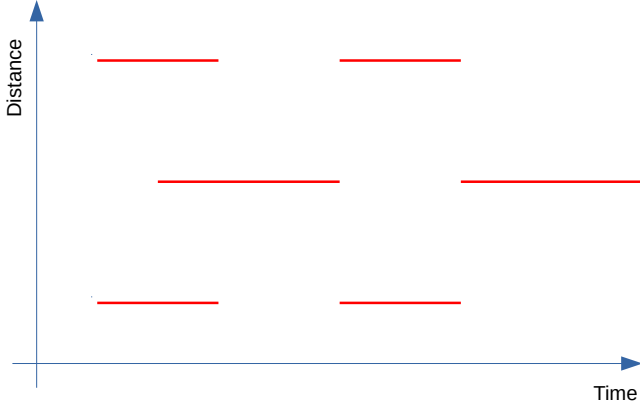


Fig. 5. Feasible Set Imposed by Traffic Lights

III. PRELIMINARIES ON MBRL

The nonlinear, stochastic, time-invariant system is considered in this work:

$$\begin{aligned} x_{t+1} &= f(x_t, u_t, w_t) \\ x_t &\in \mathcal{X} \subseteq \mathbb{R}^n, t \in \mathbb{N}_+ \\ u_t &\in \mathcal{U}(x_t) \subseteq \mathbb{R}^m, t \in \mathbb{N}_+ \\ w_t &\in \mathcal{W} \subseteq \mathbb{R}^p, t \in \mathbb{N}_+. \end{aligned} \quad (5)$$

Here, x_t , u_t and w_t are the state, control, and uncertainty at time t . \mathcal{X} and \mathcal{U} are the feasible sets for states and inputs, respectively. The uncertainties are assumed to be independent and identically distributed (i.i.d.).

Let $\pi : \mathcal{X} \rightarrow \mathcal{U}$ be an feasible deterministic policy and Π be the set of all feasible deterministic policies. The objective of the OCP is to reach the goal set $\mathcal{G} \subseteq \mathbb{R}^n$ while finding the optimal policy π^* that minimizes the expectation of the discounted sum of the costs defined as follows:

$$\begin{aligned} \pi^* &= \operatorname{argmin}_{\pi \in \Pi} \eta(\pi), \text{ where} \\ \eta(\pi) &= \mathbb{E}_{w_t} \left[\sum_{t=0}^{\infty} \gamma^t c(x_t, u_t) \right], \\ \text{where } u_t &= \pi(x_t). \end{aligned} \quad (6)$$

Here, γ is the discount factor that prioritizes the immediate rewards and ensures the sum over the infinite horizon remains finite.

As in [24], the following assumption is made regarding the cost function.

Assumption III.1 (Costs). *The cost is zero for the states inside the goal set \mathcal{G} and positive for the states outside, i.e. $\exists \epsilon > 0$ such that $c(x, u) > \epsilon \mathbb{I}_{\mathcal{G}^C(x)}$ where \mathbb{I} is the indicator function and \mathcal{G}^C is the complement of the goal set \mathcal{G} .*

As in [22], [24], [34], the following definitions are given.

Definition III.1 (Robust Control Invariant Set). *A set $\mathcal{C} \subseteq \mathcal{X}$ is said to be a robust control invariant set for the system Eqn. (5) if for all $x(t) \in \mathcal{C}$, there exists a $u(t) \in \mathcal{U}$ such that $f(x(t), u(t), w(t)) \in \mathcal{C}$, for all $w(t) \in \mathcal{W}$ and $t \in \mathbb{N}_+$.*

Definition III.2 (Robust Successor Set $\text{Suc}(\mathcal{S})$). *For a given set \mathcal{S} , its robust successor set $\text{Suc}(\mathcal{S})$ is defined as*

$$\begin{aligned} \text{Suc}(\mathcal{S}) &= \{x' \in \mathbb{R}^n : \exists x \in \mathcal{S}, \exists w \in \mathcal{W} \\ &\text{such that } x' = f(x, \pi(x), w)\}. \end{aligned} \quad (7)$$

Definition III.3 (Robust Reachable Set $\mathcal{R}_N(x_0^j)$). *For a given initial state x_0^j , the N -step robust reachable set $\mathcal{R}_N(x_0^j)$ of the system defined in Eqn. (5) in a closed loop policy π at iteration j is defined recursively as*

$$\begin{aligned} \mathcal{R}_{i+1}^\pi(x_0^j) &= \text{Suc}(\mathcal{R}_i^\pi(x_0^j)) \cap \mathcal{X}, \\ \mathcal{R}_0^\pi(x_0^j) &= x_0^j, \end{aligned} \quad (8)$$

where $i = 0, 1, \dots, N-1$.

Definition III.4 (Safe Set). *The safe set \mathcal{SS}^j contains the full evolution of the system at iteration j ,*

$$\mathcal{SS}^j = \left\{ \bigcup_{k=0}^{\infty} \mathcal{R}_k^\pi(x_0^j) \bigcup \mathcal{G} \right\}. \quad (9)$$

As shown in [22], the exact form of the safe set in 9 is a robust control invariant set. As calculating its exact form is intractable, especially for high dimensional nonlinear system, it is, in practice, approximated as

$$\widetilde{\mathcal{SS}}^j = \bigcup_{k \in \mathcal{M}^j} x^k, \quad (10)$$

where $x^k = \{x_t^k : t \in \mathbb{N}_+\}$ is the trajectory at iteration k , and $\mathcal{M}^j = \{k \in [0, j) : \lim_{t \rightarrow \infty} x_t^k \in \mathcal{G}\}$ is the set of indices of which the trajectories were successfully driven to the goal. As the safe set in this work is constantly evolving during training, the iteration index j will be neglected in the remaining work.

For any policy π , the value function $V^\pi : \mathcal{X} \rightarrow \mathbb{R}$, the Q function $Q^\pi : \mathcal{X} \times \mathcal{U} \rightarrow \mathbb{R}$ and the advantage function $A^\pi : \mathcal{X} \times \mathcal{U} \rightarrow \mathbb{R}$ are defined as follows:

$$V^\pi(x_t) = \begin{cases} \mathbb{E}_\pi \left[\sum_{i=t}^{\infty} \gamma^{i-t} c(x_i, u_i) | x_t \right], & x_t \in \mathcal{SS} \\ \infty, & \text{otherwise.} \end{cases} \quad (11)$$

$$Q^\pi(x_t, u_t) = \begin{cases} \mathbb{E}_\pi \left[\sum_{i=t}^{\infty} \gamma^{i-t} c(x_i, u_i) | x_t, u_t \right], & x_t \in \mathcal{SS} \\ \infty, & \text{otherwise.} \end{cases} \quad (12)$$

$$A^\pi(x_t, u_t) = Q^\pi(x_t, u_t) - V^\pi(x_t). \quad (13)$$

IV. PROPOSED METHOD

In this work, an off-policy model-based deep reinforcement learning algorithm with approximated safe set is proposed. At any given time t during policy execution, the following

trajectory optimization problem with a receding horizon of H steps is solved:

$$\begin{aligned} \min_{\{\tilde{u}_k\}_{k=t}^{t+H-1}} \mathbb{E} & \left[\sum_{k=t}^{t+H-1} \gamma^{k-t} c(\tilde{x}_k, \tilde{u}_k) + \gamma^H V^\pi(\tilde{x}_{t+H}) \right] \\ \text{s.t. } & \tilde{x}_{k+1} = f(\tilde{x}_k, \tilde{u}_k, w_k) \\ & \tilde{x}_t = x_t \\ & \tilde{x}_k \in \mathcal{X}, k = t, \dots, t+H-1 \\ & \tilde{x}_{t+H} \in \widetilde{\mathcal{SS}} \\ & \tilde{u}_k \in \mathcal{U}, k = t, \dots, t+H-1, \end{aligned} \quad (14)$$

where \tilde{x} and \tilde{u} are the variables for states and control actions in the predicted trajectory. Compared to the formulation in [19], the state \tilde{x}_k and action \tilde{u}_k are explicitly constrained to be within the feasible region in the receding horizon and the terminal state \tilde{x}_{t+H} to be within the safe set $\widetilde{\mathcal{SS}}$. With the presence of uncertainties in the dynamic system, solving the exact form of the above stochastic optimization problem can be challenging. In [21], [23], [24], Cross Entropy Method (CEM) is used to solve the problem with unknown dynamics as a chance constraint problem. In Section II-B, techniques will be discussed to simplify and solve the optimization in the eco-driving problem.

As most of the model-based deep reinforcement learning methods with trajectory optimization in literature learns the value function as the terminal cost for the MPC [19]–[21], [24], the learning algorithm becomes on-policy. While the trajectory optimization increases the sample efficiency and helps exploration [19], solving the trajectory optimization problem makes each data sample more computationally expensive. As a result, the training wall time is not necessarily reduced. In this work, the off-policy Q-learning [35] is instead proposed. To use the learned Q function in trajectory optimization, the following equation needs to be solved:

$$\min_{\{\tilde{u}_k\}_{k=t}^{t+H-1}} \mathbb{E} \left[\sum_{k=t}^{t+H-1} \gamma^{k-t} c(\tilde{x}_k, \tilde{u}_k) + \gamma^H Q_\theta^\pi(\tilde{x}_{t+H}, \tilde{u}_{t+H}) \right], \quad (15)$$

where Q_θ^π is the approximated Q function parametrized by θ . Compared to solving Eqn.(14), solving Eqn. (15) requires one extra computational step:

$$V^\pi(\tilde{x}_{t+H}) = \min_{\tilde{u}_{t+H}} Q_\theta^\pi(\tilde{x}_{t+H}, \tilde{u}_{t+H}). \quad (16)$$

Depending on the dimension of the problem, solving Eqn. (16) can be computationally intractable, especially for online control. Several algorithms, e.g. DDPG, TD3 and dueling network [36] are proposed to obtain the value function from the Q function. In this work, the off-policy actor-critic algorithm TD3 is used since it reduces the overestimation and is shown to be more stable than DDPG. Specifically, with the sample (x_j, u_j, c_j, x'_j) from the experience replay buffer \mathcal{D} [29], the target for the Q function during training is constructed as follows,

$$y_j = c_j + \gamma \max_{i=1,2} Q_{\theta'_i}(x'_j, u'_j), \quad (17)$$

$$u'_j = \pi_{\phi'}(x'_j). \quad (18)$$

Here, Q_{θ_1} and Q_{θ_2} are two independently trained critic networks. $Q_{\theta'_1}$ and $Q_{\theta'_2}$ are the corresponding target networks. π_ϕ and $\pi_{\phi'}$ are the actor network and its target network, respectively. The critics are then updated following

$$\begin{aligned} \theta_i \leftarrow \theta_i - \alpha \nabla_{\theta_i} & \left[\frac{1}{N} \sum_{j=1}^N (y_j - Q_{\theta_i}(x_j, u_j))^2 \right], i = 1, 2, \\ & \{(x_j, u_j, c_j, x'_j) \sim \mathcal{D}\}_{j=1}^N. \end{aligned} \quad (19)$$

where α is the learning rate, and N is the batch size.

In the off-policy learning algorithm used here, the behavior policy is the trajectory optimization where state and action constraints within the receding horizon are satisfied thanks to the constrained optimization formulation. However, the trained actor π_ϕ makes decisions solely based on the Q function. The resulting mismatch between the distribution of state-action pairs induced by the actor π_ϕ and that collected by the behavior policy results in extrapolation error leading to unstable training [27]. As an example in the eco-driving problem, the trajectory optimization ensures the power is solely generated from ICE when the battery *SoC* is at the lower limit SoC^{\min} . Accordingly, no state-action pair resembling low *SoC* and high motor torque can be collected, which leads to an extrapolation in the Q function near the region. The error can eventually cause unstable training or inferior performance.

To address the extrapolation error induced by the mismatch in distributions, Batch Constrained Q-learning (BCQ) [28] originally proposed for offline reinforcement learning is used. Here, a generative model, specifically a Variational Autoencoder (VAE) [37], $G_\omega(x)$ is trained to resemble the state-action distribution in the experience replay buffer. The background on VAE and the training objective are covered in Appendix A. Note that samples from the generative model $a' \sim G_\omega(x')$ should ideally match the distribution collected by the behavior policy. Instead of selecting action following Eqn. (18), the action is now selected as

$$u'_j = \underset{u_{j,k} + \xi_\phi(x_j, u_{j,k}, \Phi)}{\operatorname{argmin}} \left[\max_{i=1,2} Q_{\theta'_i}(x'_j, u_{j,k} + \xi_\phi(x_j, u_{j,k}, \Phi)) \right], \quad (20)$$

$$\{u_{j,k} \sim G_\omega(x'_j)\}_{k=1}^n.$$

Here n is the hyperparameter that is the number of actions sampled from the generative model. The action u' used for the target value for the Q function is selected as the best among the n sampled ones. Note that there is no longer an actor network mapping from state to action. Instead, to ensure the agent can learn on top of the actions sampled from the generative model imitating the behavior policy from the experience buffer, a perturbation network ξ_ϕ whose output is clipped between $[-\Phi, \Phi]$ is trained. The perturbation network ξ_ϕ is updated by deterministic policy gradient theorem from [38] as

$$\phi \leftarrow \phi - \alpha \nabla_\phi \left[\frac{1}{N} \sum_{j=1}^N Q_{\theta_1}(x_j, u_j + \xi_\phi(x_j, u_j, \Phi)) \right]. \quad (21)$$

To reduce the accumulating error from bootstrapping, all the target networks are updated with a slower rates as

$$\theta'_i \leftarrow \tau \theta_i + (1 - \tau) \theta'_i, \quad i = 1, 2, \quad (22)$$

$$\phi' \leftarrow \tau \phi + (1 - \tau) \phi', \quad (23)$$

where τ is a constant on the order of 10^{-3} to 10^{-1} .

In [23], [24], the safe set is approximated by kernel density estimation, which typically works well only for problems in low dimensions. Here, we extend the approximation to high-dimensional setting by using deep generative models. Following the notion in [23], the safe set is approximated as

$$\widetilde{\mathcal{S}} = \{x : p_\psi(x) \geq \delta\}, \quad (24)$$

where $p_\psi : \mathcal{X} \rightarrow [0, 1]$ is the probability that a state is inside the safe set parametrized by ψ , and the constant δ regulates how exploratory the controller is. Note that the generative model used for safe set approximation needs to model the probability explicitly and can be slow in sampling, whereas the generative model resembling the distribution of state-action pairs in the experience replay needs to be fast in sampling while the explicit probability is not required.

Due to the aforementioned consideration, autoregressive model with Long Short-term Memory (LSTM) [39] is used. The description of the model as well as the training objective is included in Appendix B. In Sec.V, the use of the autoregressive model in the application of eco-driving is motivated as the dimension of the problem can get large once the future conditions are sampled discretely.

In summary, Safe Model-based Off-policy Reinforcement Learning (SMORL) is proposed. The algorithm builds on SAVED [23] and extends it to be an off-policy algorithm with the methods proposed in BCQ. The detailed step-by-step algorithm is included in Algorithm 1.

V. IMPLEMENTATION DETAILS

A. Trajectory Optimization

Specific to the eco-driving problem, the state vector x_t is defined as a vector with 88 states. A description of the states are listed in Tab. I. Here, the first seven elements of the state vector are the battery SoC , the vehicle speed v_{veh} , the current speed limit v_{lim} , the next speed limit v'_{lim} , the distance to the next speed limit s_{lim} , the distance to the upcoming traffic light s_{tls} and the total remaining distance s_{rem} . The remaining 81 elements are the sampled upcoming traffic light status in the next 80 seconds x_{tfc} . For example, if the upcoming traffic light has 20 seconds remaining for the current red phase and will remain in green for the rest of the 80 seconds, the first 21 elements of the sampled upcoming traffic light status are 0, and the rest are set to 1. Compared to the manually extracted feature representation in [16], the sampled representation reduces the discontinuity and results in a better performance.

As the vehicle considered in this study is assumed equipped with connected features, e.g. advanced mapping and V2I connectivity, and surrounding vehicles are not included in the study, it is assumed that the ego vehicle can deterministically predict the uncertainties from driving conditions within the

receding horizon in this study. Sun et al. [6] suggests by formulating the problem as a chance constraint or a distributionally robust optimization problem, uncertainties in SPaT can be considered without additional computational load.

In Eqn. (4), the receding horizon H is in time domain. While it is easier to incorporate the time-based information such as SPaT received from V2I communication in time domain, an iterative dynamic look-ahead process is required to process any distance-based route feature, such as speed limits, grade, traffic light and stop sign locations. For example, the controller requires the speed limits as the constraints to generate speed trajectory while the speed limits can change based on the distance travelled by the speed trajectory. In this study, the value and Q functions are learned in time domain for the ease of integration with time-based traffic simulator, while the trajectory optimization is conducted in spatial domain.

As SPaTs and speed limits do not depend on the decision made by the ego vehicle in distance domain, they are incorporated into the optimization problem as constraints, and only the vehicle speed, battery SoC and the time at which the vehicle reaches the given distance are considered as the state in the trajectory optimization. Define the optimization state $z \in \mathcal{Z} \subseteq \mathbb{R}^3$ as

$$z_s = [v_{veh,s}, SoC_s, t_s]^T. \quad (25)$$

Here, s is the index in the discretized spatial domain with $\Delta s = 10m$, and the dynamics of z in time and spatial domains are converted following

$$\frac{\Delta z}{\Delta s} = \frac{\Delta z}{\Delta t} \frac{\Delta t}{\Delta s} = \frac{\Delta z}{\Delta t} \frac{1}{v_{veh}}. \quad (26)$$

As a result, the trajectory optimization is formulated as

$$\min_{\{\tilde{u}\}_{k=s_t}^{s_t+H_s-1}} \sum_{k=s_t}^{s_t+H_s-1} \gamma^{t_k} c(\tilde{z}_k, \tilde{u}_k) + \gamma^{t_{H_s}} V^\pi(\mathcal{G}(x_t, z_{H_s})) \quad (27a)$$

where:

$$c(\tilde{x}_k, \tilde{u}_k) = (\lambda \dot{m}_{fuel,k} + (1 - \lambda)) \frac{\Delta s}{v_{veh,k}} \cdot \mathbb{I}[s_k < s_{total}] \quad (27b)$$

$$\text{s.t. } SoC_{k+1} = f_{batt,s}(\tilde{z}_k, \tilde{u}_k) \quad (27c)$$

$$v_{veh,k+1} = f_{veh,s}(\tilde{z}_k, \tilde{u}_k) \quad (27d)$$

$$T_{eng}^{\min}(\omega_{eng,k}) \leq T_{eng,k} \leq T_{eng}^{\max}(\omega_{eng,k}) \quad (27e)$$

$$T_{bsg}^{\min}(\omega_{bsg,k}) \leq T_{bsg,k} \leq T_{bsg}^{\max}(\omega_{bsg,k}) \quad (27f)$$

$$I^{\min} \leq I_k \leq I^{\max} \quad (27g)$$

$$SoC^{\min} \leq SoC_k \leq SoC^{\max} \quad (27h)$$

$$0 \leq v_{veh,k} \leq v_{lim,k} \quad (27i)$$

$$(t_k, s_k) \notin \mathcal{S}_{red} \quad (27j)$$

$$\mathcal{G}(x_t, z_{H_s}) \in \widetilde{\mathcal{S}}. \quad (27k)$$

Here, s_t is the spatial index corresponding to the distance the ego vehicle has traveled at the time t . $H_s = 20$ is the prediction step in spatial domain, making the total prediction horizon 200 m. $\mathcal{G} : \mathcal{X} \times \mathcal{Z} \rightarrow \mathcal{X}$ is the function that takes the full state x_t and the terminal optimization state z_{H_s}

Algorithm 1: Safe Model-based Off-policy Reinforcement Learning (SMORL)

Initialize Q-networks Q_{θ_1} , Q_{θ_2} independently, and duplicate target networks $Q_{\theta'_1}$, $Q_{\theta'_2}$.
Initialize the perturbation network ξ_ϕ , its target network ξ'_ϕ and VAE $G_\omega = \{E_{\omega_1}, D_{\omega_2}\}$.
Initialize the experience replay buffer \mathcal{D} .
Collect N_0 successfully executed trajectories with a baseline controller and initialize the safe set $\widetilde{\mathcal{SS}}$.
for $n_{iter} \in 1, \dots, N_{iter}$ **do**
 while j^{th} trajectory NOT finished **do**
 Select control action u_t by solving trajectory optimization in Eqn. (14).
 Sample mini-batch of N transitions (x, u, c, x') from \mathcal{D} .
 For each transition, sample n actions u'_j from $G_\omega(x')$ and n perturbations from $\xi_\phi(x', u', \Phi)$.
 Update the critic networks Q_{θ_1} , the target networks $Q_{\theta'_1}$ following Eqn. (19) and Q_{θ_2} , $Q_{\theta'_2}$ following Eqn. (22).
 Update perturbation network ξ_ϕ following Eqn. (21).
 Update VAE G_ω by maximizing Eqn. (30).
 end
 if $x_T \in \mathcal{G}$ **then**
 Push the trajectory $\{(x_t, u_t, c_t, x_{t+1})\}^T$ to \mathcal{D} .
 Update the safe set \mathcal{SS} with minibatches sampled from \mathcal{D} following Eqn. (32).
 end
end

TABLE I
THE STATE AND ACTION SPACES OF THE ECO-DRIVING PROBLEM

	Variable	Description
\mathcal{X}	$SoC \in \mathbb{R}$	Battery SoC
	$v_{veh} \in \mathbb{R}$	Vehicle velocity
	$v_{lim} \in \mathbb{R}$	Speed limit at the current road segment
	$v'_{lim} \in \mathbb{R}$	Upcoming speed limit
	$d_{tfc} \in \mathbb{R}$	Distance to the upcoming traffic light
	$d'_{lim} \in \mathbb{R}$	Distance to the road segment of which the speed limit changes
	$d_{rem} \in \mathbb{R}$	Remaining distance of the trip
	$x_{tfc} \in \{0, 1\}^{81}$	Sampled status of the upcoming traffic light
\mathcal{U}	$T_{eng} \in \mathbb{R}$	Engine torque
	$T_{bsg} \in \mathbb{R}$	Motor torque
	$T_{brk} \in \mathbb{R}$	Equivalent brake torque

and determines the predicted terminal full state $\tilde{x}_{t+t_{H_s}}$. For example, suppose there are 15 seconds left in the current green phase and t_{H_s} in the optimization state is 10 seconds, i.e. it takes 10 seconds for the ego vehicle to travel the future 200 m, there will be 5 seconds left in the current green phase at the end of the prediction horizon. The trajectory optimization problem is solved by Deterministic Dynamic Programming (DDP) [40]. The optimal deterministic policy $\mu_k^* : \mathcal{Z} \rightarrow \mathcal{U}$, $k = 1, 2, \dots, H_s - 1$, along with the optimal cost-to-go function $\mathcal{J}_k : \mathcal{Z} \rightarrow \mathbb{R}$, $k = 1, 2, \dots, H_s$ can be calculated through backward recursion as

$$\mathcal{J}_{H_s}(z) = V^\pi(\mathcal{G}(x_t, z)) + \mathcal{P}_N(z), \quad (28a)$$

$$\mathcal{F}_k(z, u) = c(z, u) + \mathcal{P}_k(z) + \mathcal{J}_{k+1}(\mathcal{G}_k(x, u)), \quad (28b)$$

$$\mu_k^* = \underset{\mu_k}{\operatorname{argmin}} \mathcal{F}_k(z, \mu_k(z)), \quad (28c)$$

$$\mathcal{J}_k(z) = \mathcal{F}_k(z, \mu_k^*(z)). \quad (28d)$$

Here, $\mathcal{F} : \mathcal{Z} \times \mathcal{U} \rightarrow \mathbb{R}$ is the cost-to-go associated with a given immediate action and then the optimal policy. $\mathcal{P}_k : \mathcal{Z} \rightarrow \mathbb{R}$

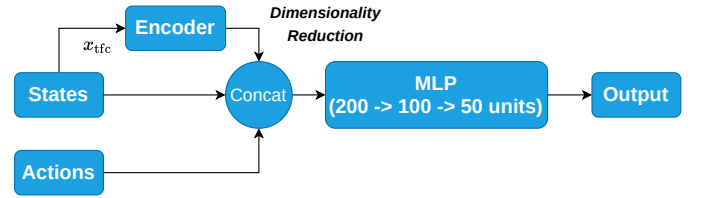


Fig. 6. The Network Architecture of the Value and Q Functions.

and $\mathcal{P}_N : \mathcal{Z} \rightarrow \mathbb{R}$ are penalty functions introduced to ensure no constraint violation in the predicted trajectory.

Solving Eqn. (28) is computationally intensive yet highly parallelizable. Considering onboard GPU is readily available nowadays on self-driving vehicles, a CUDA-based Parallel DDP (PDDP) solver in [41] is used in this work. In the cases where the stochasticity within the prediction horizon cannot be ignored, other gradient-free optimization methods, such as CEM or random shooting method [42], can be used as the trajectory optimizer.

B. Q Learning

Fig. 6 shows the architecture of the neural network associated with the Q-learning. Upon receiving the state vector, the sampled traffic light status w_{tfc} are fed to a pre-trained autoencoder with Multilayer Perceptron (MLP) of size (81, 100, 5, 100, 81) for dimensionality reduction. The remaining states along with the actions are concatenated with the latent states from the encoder, and subsequently fed into another MLP of size (200, 100, 50) to output the Q function for critic and perturbation for actor. The critic and the actor do not share parameters in this work.

To accelerate the training and improve generalizability, the state of the vehicle is randomized for every 50 steps in simulation. When the domain randomization occurs, the battery SoC and the vehicle velocity $v_{veh,t}$ are sampled

from uniform distributions $\text{Uniform}(SoC^{\min}, SoC^{\max})$ and $\text{Uniform}(0, v_{\lim, t})$, respectively. To guarantee feasibility during the trip, the domain randomization is disabled 200m within signalized intersections or 1000m within the final destination.

C. Safe Set Approximation

In the eco-driving problem, two types of constraints can induce feasibility issue, namely, the battery terminal SoC constraint and the constraint imposed by traffic rules at signalized intersections. For the first case, the goal set is considered not reached when the vehicle is near the destination and it cannot sufficiently charge the battery back to SoC^T in the remaining distance. For the second case, the trip is considered failed when the vehicle breaks traffic rules at signalized intersections, and infeasibility occurs when the vehicle speed is too high and there is not enough distance to brake to stop in front of a traffic light in red or stop sign. A conservative low speed controller that only uses ICE is used to collect the initial data for the experience replay buffer. During training, only samples from the trips that reach the goal set without violating any constraints are added to the experience replay buffer.

In the eco-driving problem, the sampled traffic light x_{tfc} is binary, while the other variables are continuous. As the PDDP solver also discretize the continuous state space, we consider the loss of accuracy with the same discretization is acceptable. The discretized states as in one-hot form in each dimension are fed into a LSTM network with 50 units sequentially as shown in Fig. 11. The outputs from LSTM are then masked according to the number of categorical classes in each dimension. Finally, the softmax operator ensures the outputs to be proper conditional probability distribution. As an alternative to LSTM, Causal 1D Convolutional Neural Networks (Causal Conv1D) [43] was also implemented as the network for the autoregressive model. The key difference is that the states in all dimensions can be fed into Causal Conv1D in parallel, whereas each dimension needs to be fed into LSTM sequentially. For applications with long sequence, Causal Conv1D can be more efficient and accurate [44]. For the specific problem, Causal Conv1D shows no noticeable advantage over LSTM in either accuracy or inference speed. As a result, LSTM is chosen as it has less hyperparameters.

When the receding horizon (200m) in this study is longer than the critical braking distance [16], the vehicle will never violate any constraints imposed by signalized intersections. Nevertheless, using the safe set to constrain the terminal state is still essential for the following reason. At the last step of the receding horizon, the value function $V^\pi(\tilde{x}_{t+\Delta t_{H_s}})$ needs to be evaluated numerically for trajectory optimization. Since only the data from the safely executed trips is added into the buffer and there is no penalty mechanism for the constraint violation, the estimation of the critic network is valid only within the safe set and is subject to extrapolation error outside. Although the long receding horizon ensures the feasibility of the actual trajectory regardless of the use of safe set, the training is subject to instability and the learned performance can be significantly deteriorated without the constraint from the safe set.

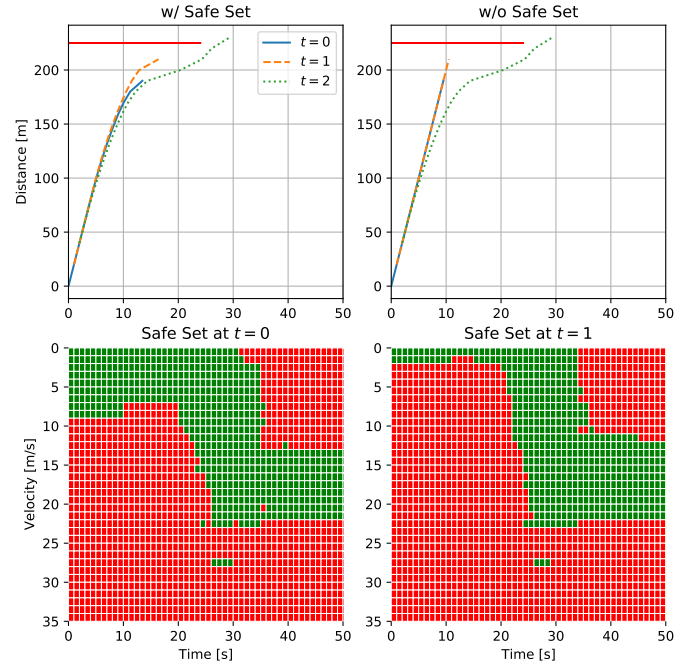


Fig. 7. The Effect Of the Safe Set on Trajectory Optimization.

This effect is shown in Fig. 7. Here, the two subplots on top show the optimized trajectories with and without the use of safe set, respectively. The three curves in each plot are the trajectories from the optimizer at three consecutive seconds. During the first two seconds, the vehicle is more than 200m away from the traffic light, and thus the constraint from Eqn. (4k) is not considered in the trajectory optimization. The subplots on the bottom show the safety status of the terminal state in the dimension of the vehicle velocity and the time at which it reaches the end of the receding horizon before the signalized intersection appears in the receding horizon. Here, green means the state is considered safe, i.e. $p_\psi(x) \geq \delta$, and red otherwise. Although the actual trajectories, with or without safe set, are able to slow down in time to avoid trespassing the red light thanks to the sufficiently long receding horizon, the terminal state without the safe set constraint has a speed of 20m/s with 20m left before a red light, which is clearly unsafe. Meanwhile, comparing the bottom two subplots, the terminal velocity constrained by the safe set progressively reduces as the vehicle approaches the intersection in red phase. In addition, given speed limit here is set to $v_{\lim} = 22\text{m/s}$, any state with velocity higher than 22m/s is considered unsafe. It can be noticed that the red region on the top right corners are incorrectly considered as unsafe (false positive). This is because, by optimality, the agent rarely crosses an intersection in green phase with low speed, therefore, these false positive regions do not affect the performance.

As a summary for all the implementation details, the hyperparameters are listed in Tab. II.

VI. RESULTS

Both the PDDP optimizer and the neural network training requires GPU. To get the results to be shown, the training took

TABLE II
HYPERPARAMETERS OF THE Q LEARNING AND SAFE SET ESTIMATION

Parameter	Value
Weighting factor between fuel and time, λ	0.45
Discount factor, γ	0.995
Optimizer	Adam
Learning rate, α	1e-4
Experience buffer size	2e5
Batch size, N	256
Target network update rate, τ	1e-3
Exploration rate, ϵ	0.2
Perturbation range in physical unit, Φ	30 Nm
Sampled actions from the VAE decoder, n	10
Steps per domain randomization	50
LSTM size for the safe set	50

TABLE III
FUEL ECONOMY, AVERAGE SPEED AND SOC VARIANCE FOR BASELINE, MODEL-FREE DRL, SMORL AND WAIT-AND-SEE SOLUTIONS

	Baseline	MFDRL	SMORL	Wait-and-See
Fuel Economy mpg	32.4	40.8	41.6	47.5
Speed Mean m/s	14.1	12.5	14.0	14.5
<i>SoC</i> Variance % ²	12.1	18.2	52.6	22.6

24 hours on a node with a NVIDIA Volta V100 GPU and 2.4GHz Intel CPU from Ohio Supercomputer Center [45]. As domain randomization is used during training, 5 trips out of the 1000 randomly generated trips are repeatedly selected for every 25 training episodes to evaluate the performance of the controller and to quantify the progress of training. During evaluation, domain randomization and epsilon greedy are both deactivated. Fig. 8 shows the evolution of the total costs, fuel economy and average speed of the 5 evaluation trips. Comparing to the model-free on-policy method in [16], which takes 80,000 episodes to converge, the sample efficiency of the off-policy model-based method is significantly improved. In the meantime, with the constrained optimization formulation and the safe set, the training quickly learns to respect the constraints imposed by the terminal *SoC* and signalized intersections. Furthermore, the fact that the agent does not need any extrinsic penalty from constraint violation and is still capable of learning to operate within the safe region significantly simplifies the design and tuning process as deployed in the previous reinforcement learning attempts on eco-driving [14]–[16].

Statistically, the performance of the agent trained with SMORL is compared against the three other controllers, a baseline EDM driver representing a human driver with comparable average speed [46], the Model-free DRL (MFDRL) agent proposed in [16] and the wait-and-see solution. The wait-and-see solution assumes the speed limits and the sequences of all traffic lights of the entire trip are known *a priori*, and it is solved by PDDP solver as well. Despite being non-causal and computational intractable for online implementation, the solution serves as the upper bound for the causal control strategies. The four strategies are evaluated on the 100 random trips as shown in Fig. 4, and the fuel economy, average speed and variance of the battery *SoC* are listed in Tab. III.

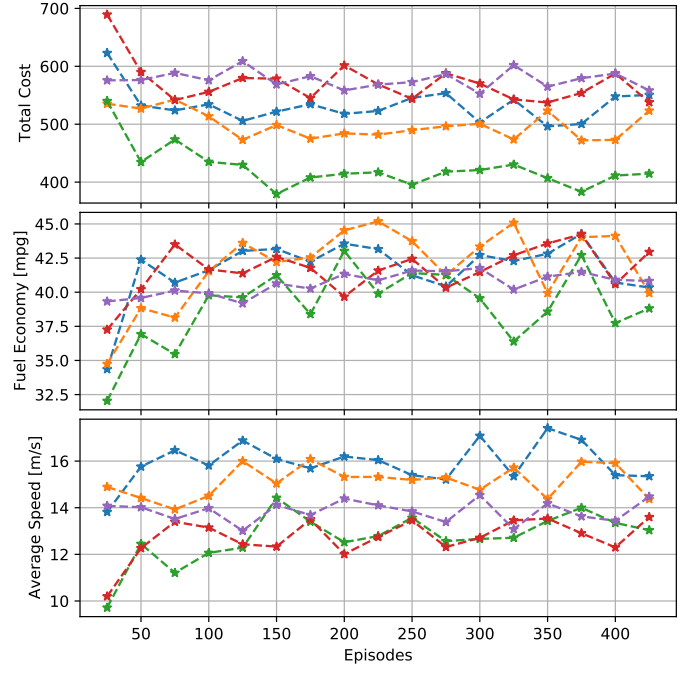


Fig. 8. The Evolution of the Total Costs, Fuel Economy, and Average Speed of the 5 Evaluation Trips.

Here, the proposed model-based method has a dominant performance in average speed and fuel economy compared to the previously trained MFDRL strategy, which is primarily due to two aspects. First, the online trajectory optimization solved by PDDP guarantees the global optimality within the receding horizon. Compared to the actions generated from the one-step stochastic policy from neural network, the solution from trajectory optimization is more accurate and reliable. Second, the fact that there is no extrinsic penalty to assist constraint satisfaction ensures that the agent focuses on learning only the objective of the OCP formulation, i.e. weighted sum of the trip time and fuel consumption, instead of a carefully designed yet delicate surrogate learning objective. Compared to the baseline EDM driver, SMORL agent consumes 21.8% less total fuels while maintaining a comparable average speed. The benefit in fuel economy is achieved by avoiding unnecessary acceleration events and by taking advantage of a wider range of battery capacity as indicated by the higher *SoC* variance.

In Fig. 9, the mean and standard deviation of the vehicle speed and the fuel economy of each trip are plotted against the traffic light density. As the wait-and-see solution calculates the global optimal solution with the knowledge of the full trip, it is able to navigate among the traffic lights accordingly, as indicated by the non-increasing standard deviation of the vehicle speed. In fact, the overall fuel economy increases as the traffic density increases. This can be due to the fact that when there are more traffic lights, the vehicle is forced to operate with a lower speed and lower fuel consumption condition. On the other hand, as the baseline driver has limited line-of-sight [46] and only the SPaT of the upcoming traffic light is available to SMORL, the standard deviation of the vehicle speed increases and the fuel economy decreases as the traffic

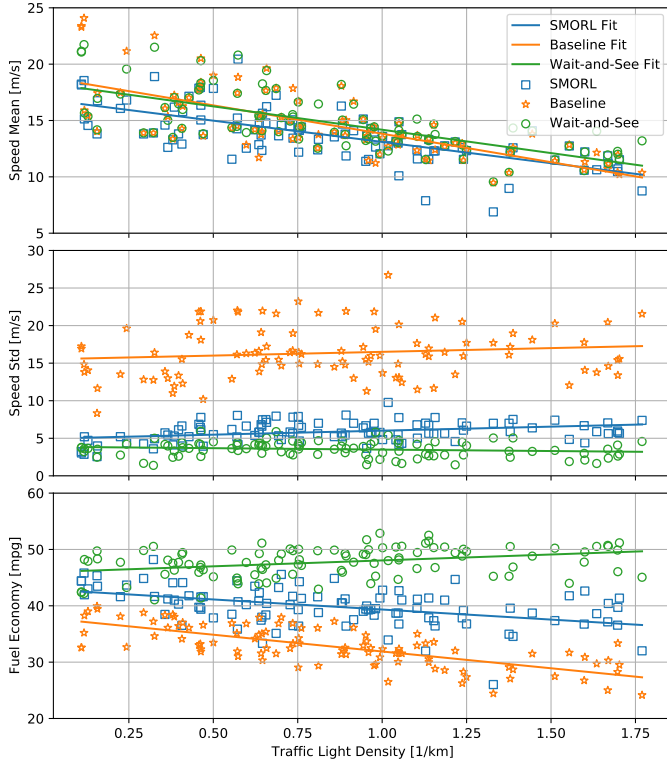


Fig. 9. The Variation of the Average Speed and the Fuel Economy against Traffic Light Density for Baseline, SMORL and Wait-and-see Solution

light density increases. Nevertheless, as indicated by the slope of the fitted curve, the fuel economy of SMORL is slightly less affected by the increase of the traffic light density compared to the baseline.

Fig. 10 shows the comparison among the baseline, SMORL and the wait-and-see solution on a specific testing trip. For this specific trip, while trip time are within 3s, SMORL and the wait-and-see solution consume 24.7% and 40.0% less fuels compared to the baseline strategy, respectively. While SMORL demonstrates some merits similar to the wait-and-see solution, its inferiority is primarily due to the fact that only the SPaTs from the upcoming intersection is available to the controller. In this trip specifically, the wait-and-see solution deployed a constant low-speed strategy from $\sim 1,700m$ all the way till the end of the trip. Although it was behind the other two at the intersection at $4,300m$ by one red phase, it was able to eventually catch by not having to waste anytime at stop. While knowing the SPaTs from the entire trip is unrealistic and subject to uncertainties, the SMORL was able to save a significant amount of fuel compared to the baseline by 1) decelerating ahead of time, 2) decelerating with more energy recuperation using electric motor, 3) avoiding unnecessary high speed within the connectivity range. Additional comparison among the three strategies are shown in Appendix C.

VII. CONCLUSION

In this paper, a safe-critical model-based off-policy reinforcement learning algorithm SMORL is proposed. The

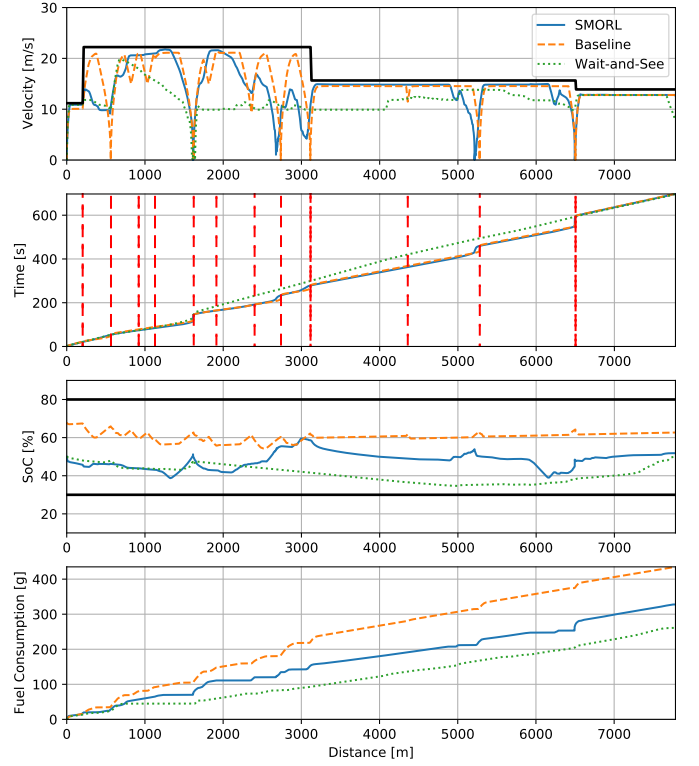


Fig. 10. The Trajectory Comparison among Baseline, SMORL and Wait-and-See.

algorithm is applied to the eco-driving problem for Connected and Automated Hybrid Electric Vehicles. Compared to the previous model-free attempts on eco-driving in the literature, the method does not require any extrinsic rewarding mechanism, and thus, greatly simplifies the design process and improves the final performance. With the online constrained optimization formulation and the approximate safe set, the learned strategy is capable of satisfying the constraints in the prediction horizon and restricting the state within the approximate safe set, which is an approximation to the robust control invariant set. The performance of the strategy trained with SMORL is compared to a baseline strategy representing human drivers' behavior over 100 randomly generated trips in Columbus, OH, US. With a comparable average speed, the strategy from SMORL consumes approximately 22% less fuel.

While the demonstration of the algorithm is on the eco-driving problem, we believe it can be applied to many other real-world problems, in particular to those with well-studied system dynamics, such as robotics and autonomous driving. Future works include 1) incorporating SPaT information broadcasted from multiple upcoming signalized intersections, 2) incorporating surrounding vehicles into the model, and accordingly update the optimal control problem, 3) releasing the deterministic assumption within the prediction horizon.

APPENDIX A VARIATIONAL AUTOENCODER

Let $X = \{x_i\}_{i=1}^N$ be some data set and Z represent a set of low-dimensional latent variables, the objective is to maximize

the marginal log-likelihood:

$$\begin{aligned} \log p(X) &= \sum_{i=1}^N \log p(x_i) = \sum_{i=1}^N \int_z \log p(x_i|z) p(z) dz \\ &= \sum_{i=1}^N \mathbb{E}_{z \sim p(z)} \log p(x_i|z), \end{aligned} \quad (29)$$

As Eqn. (29) is in general intractable, its variational lower bound is instead maximized:

$$\begin{aligned} \mathcal{L}(\omega_1, \omega_2, X) &= -D_{\text{KL}}(q_{\omega_1}(z|X) || p(z)) \\ &\quad + \mathbb{E}_{q_{\omega_1}(z|X)} [\log p_{\omega_2}(X|z)] \end{aligned} \quad (30)$$

Here, D_{KL} is the Kullback–Leibler (KL) divergence, and $p(z)$ is the prior distribution that is typically assumed to be a multivariate normal distribution. $q_{\omega_1}(z|X)$ is the posterior distribution parametrized by ω_1 . To analytically evaluate the KL divergence, the posterior is typically constructed as $\mathcal{N}(z|\mu_{\omega_1}(X), \Sigma_{\omega_1}(X))$. From a coding theory perspective, $q_{\omega_1}(z|X)$ and $p_{\omega_2}(X|z)$ can be considered as a probabilistic encoder and a probabilistic decoder, respectively.

To compute the $\nabla_{\omega_1} L(\omega_1, \omega_2, X)$, policy gradient theorem [47] or Reparametrization trick [37], [47] can be used. The latter is often used in VAE as it typically leads to a lower variance.

In practice, the encoder $q_{\omega_1}(z|X)$ and the decoder $p_{\omega_2}(X|z)$ can be any function approximator. An implementation of VAE as the generative model to sample actions can be found in <https://github.com/sfujim/BCQ>. In this work, the latent space dimension is selected to be 5, and the encoder and the decoder are both MLPs with 2 layers of 300 hidden units.

APPENDIX B AUTOREGRESSIVE MODEL WITH LSTM

For any probability distribution, the joint distribution can be factorized as a product of conditional probabilities as follow:

$$\begin{aligned} p(x) &= \prod_{i=1}^K p(x^{(i)} | x^{(1)}, \dots, x^{(i-1)}), \\ \rightarrow \log p(x) &= \sum_{i=1}^K \log p(x^{(i)} | x^{(1)}, \dots, x^{(i-1)}), \end{aligned} \quad (31)$$

where $x^{(i)}$ is the i^{th} dimension of the discrete input vector and K is the dimension of the input vector. As shown in Fig. 11, the input vector in one-hot vector form is fed to the LSTM network in sequence. The i^{th} output of the LSTM network after the softmax operation becomes a proper conditional probability $p(x^{(i)} | x^{(1)}, \dots, x^{(i-1)})$. The model is trained by minimizing the KL divergence between the data distribution sampled from the experience replay buffer and the modeled distribution:

$$\begin{aligned} &\min_{\psi} D_{\text{KL}}[p^*(x) || p_{\psi}(x)] \\ &= \min_{\psi} \mathbb{E}_{x \sim p^*(x)} [-\log p_{\psi}(x)] + \text{constant} \end{aligned} \quad (32)$$

In this work, the LSTM network has a single layer and 50 hidden size.

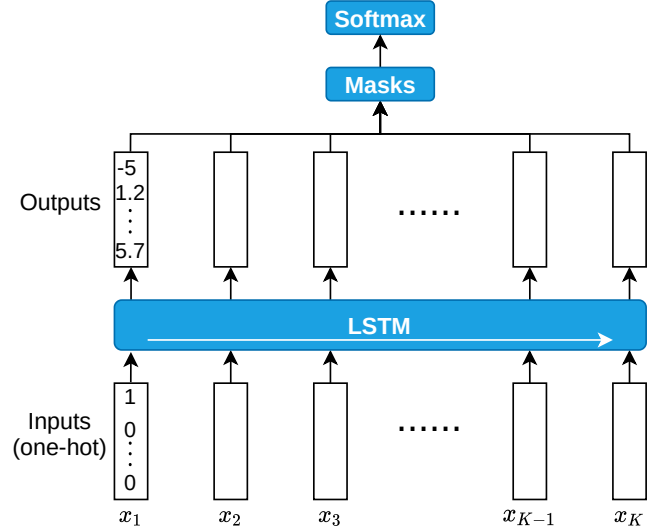


Fig. 11. The Network Architecture of Recurrent Autoregressive Model.

APPENDIX C ADDITIONAL COMPARISON AMONG STRATEGIES

Here, we show the comparison on two additional trips. The trip shown in Fig. 12 contains a large number of signaled intersections. As indicated by Fig. 9, the gap between SMORL and the baseline and the gap between the wait-and-see solution and SMORL are both amplified by the high traffic density. The trip shown in Fig. 13 has a very low traffic density and the speed limits higher. In such case, the difference between SMORL and the wait-and-see solution becomes less noticeable. Meanwhile, SMORL was still able to consume less fuel by using the capacity of the battery more efficiently.

APPENDIX D ABLATION

In this part, we compare the full SMORL algorithm with the four intermediate algorithms. All the algorithms presented below use trajectory optimization solved via PDDP solver. Tab. IV shows the difference in configuration and compare the trained final performance over the 100 trips used for testing. Here, we see that safe set and BCQ both have positive impact on the trained performance. In fact, the native combination of TD3 and trajectory optimization (Config. 2) does not provide any show any significant improvement over trajectory optimization only (Config. 1). In addition, without the use of safe set, the controller will deplete the battery SoC to SoC^{\min} at the end of the trip as the terminal state constraint cannot be considered unless with the help of extrinsic penalty.

ACKNOWLEDGMENT

The authors acknowledge the support from the United States Department of Energy, Advanced Research Projects Agency – Energy (ARPA-E) NEXTCAR project (Award Number DE-AR0000794) and Ohio Supercomputer Center.

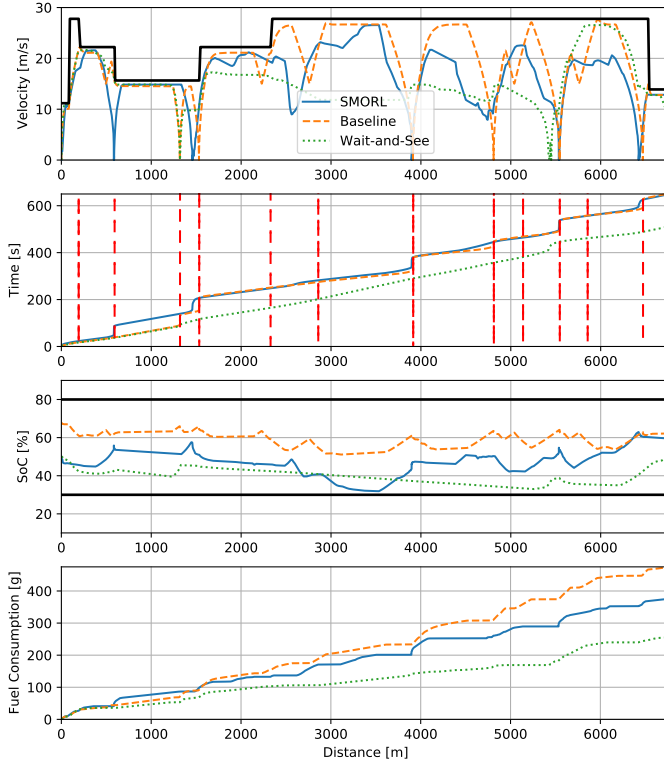


Fig. 12. Comparison for High-density Low-speed Scenario.

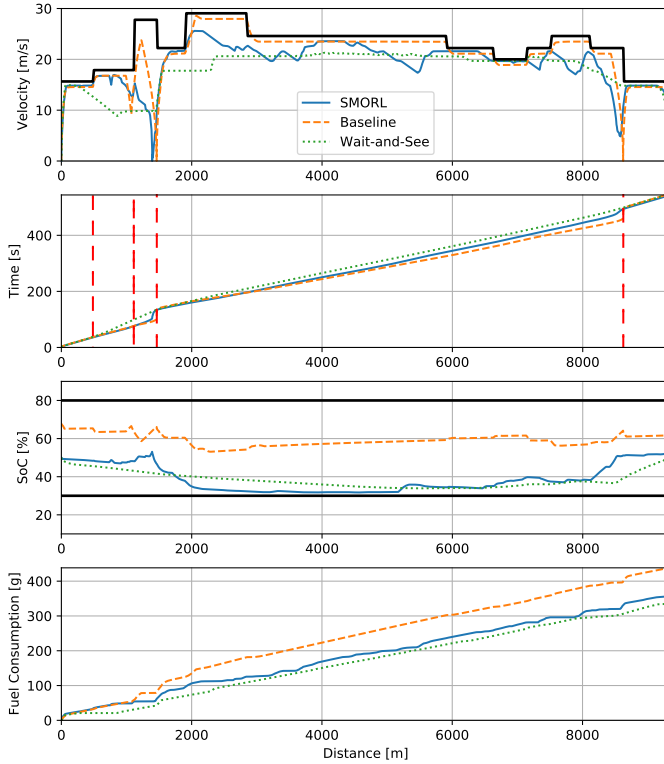


Fig. 13. Comparison for Low-density High-speed Scenario.

REFERENCES

[1] A. Vahidi and A. Sciarretta, "Energy saving potentials of connected and automated vehicles," *Transportation Research Part C: Emerging Technologies*, vol. 95, pp. 822–843, 2018.

TABLE IV
ABLATION STUDY FOR SMORL

	Safe Set	Q-learning	Fuel Economy mpg	Average Speed m/s	Normalized Cost
1		None	43.1	11.2	100
2		TD3	39.1	13.9	88.0
3	✓	TD3	39.9	13.3	90.5
4		BCQ	38.5	14.3	87.2
5	✓	BCQ	41.6	14.0	86.5

- [2] A. Sciarretta, G. De Nunzio, and L. L. Ojeda, "Optimal ecodriving control: Energy-efficient driving of road vehicles as an optimal control problem," *IEEE Control Systems Magazine*, vol. 35, no. 5, pp. 71–90, 2015.
- [3] Q. Jin, G. Wu, K. Boriboonsomsin, and M. J. Barth, "Power-based optimal longitudinal control for a connected eco-driving system," *IEEE Transactions on Intelligent Transportation Systems*, vol. 17, no. 10, pp. 2900–2910, 2016.
- [4] E. Ozatay, S. Onori, J. Wollaeger, U. Ozguner, G. Rizzoni, D. Filev, J. Michelini, and S. Di Cairano, "Cloud-based velocity profile optimization for everyday driving: A dynamic-programming-based solution," *IEEE Transactions on Intelligent Transportation Systems*, vol. 15, no. 6, pp. 2491–2505, 2014.
- [5] J. Han, A. Vahidi, and A. Sciarretta, "Fundamentals of energy efficient driving for combustion engine and electric vehicles: An optimal control perspective," *Automatica*, vol. 103, pp. 558–572, 2019.
- [6] C. Sun, J. Guanetti, F. Borrelli, and S. Moura, "Optimal eco-driving control of connected and autonomous vehicles through signalized intersections," *IEEE Internet of Things Journal*, 2020.
- [7] F. Mensing, R. Trigui, and E. Bideaux, "Vehicle trajectory optimization for hybrid vehicles taking into account battery state-of-charge," in *2012 IEEE vehicle power and propulsion conference*. IEEE, 2012, pp. 950–955.
- [8] L. Guo, B. Gao, Y. Gao, and H. Chen, "Optimal energy management for hevs in eco-driving applications using bi-level mpc," *IEEE Transactions on Intelligent Transportation Systems*, vol. 18, no. 8, pp. 2153–2162, 2016.
- [9] P. Olin, K. Aggoune, L. Tang, K. Confer, J. Kirwan, S. R. Deshpande, S. Gupta, P. Tulpule, M. Canova, and G. Rizzoni, "Reducing fuel consumption by using information from connected and automated vehicle modules to optimize propulsion system control," SAE Technical Paper, Tech. Rep., 2019.
- [10] D. Maamria, K. Gillet, G. Colin, Y. Chamaillard, and C. Nouillant, "Computation of eco-driving cycles for hybrid electric vehicles: Comparative analysis," *Control Engineering Practice*, vol. 71, pp. 44–52, 2018.
- [11] O. D. Altan, G. Wu, M. J. Barth, K. Boriboonsomsin, and J. A. Stark, "Glidepath: Eco-friendly automated approach and departure at signalized intersections," *IEEE Transactions on Intelligent Vehicles*, vol. 2, no. 4, pp. 266–277, 2017.
- [12] B. Asadi and A. Vahidi, "Predictive cruise control: Utilizing upcoming traffic signal information for improving fuel economy and reducing trip time," *IEEE Transactions on Control Systems Technology*, vol. 19, no. 3, pp. 707–714, 2011.
- [13] J. Shi, F. Qiao, Q. Li, L. Yu, and Y. Hu, "Application and evaluation of the reinforcement learning approach to eco-driving at intersections under infrastructure-to-vehicle communications," *Transportation Research Record*, vol. 2672, no. 25, pp. 89–98, 2018.
- [14] G. Li and D. Gorges, "Ecological adaptive cruise control for vehicles with step-gear transmission based on reinforcement learning," *IEEE Transactions on Intelligent Transportation Systems*, 2019.
- [15] A. Pozzi, S. Bae, Y. Choi, F. Borrelli, D. M. Raimondo, and S. Moura, "Ecological velocity planning through signalized intersections: A deep reinforcement learning approach," in *2020 59th IEEE Conference on Decision and Control (CDC)*. IEEE, 2020, pp. 245–252.
- [16] Z. Zhu, S. Gupta, A. Gupta, and M. Canova, "A deep reinforcement learning framework for eco-driving in connected and automated hybrid electric vehicles," *arXiv preprint arXiv:2101.05372*, 2021.
- [17] D. P. Bertsekas, *Dynamic programming and optimal control*. Athena scientific Belmont, MA, 2005, vol. 1, no. 3.
- [18] T. Wang, X. Bao, I. Clavera, J. Hoang, Y. Wen, E. Langlois, S. Zhang,

- G. Zhang, P. Abbeel, and J. Ba, "Benchmarking model-based reinforcement learning," *arXiv preprint arXiv:1907.02057*, 2019.
- [19] K. Lowrey, A. Rajeswaran, S. Kakade, E. Todorov, and I. Mordatch, "Plan online, learn offline: Efficient learning and exploration via model-based control," *arXiv preprint arXiv:1811.01848*, 2018.
- [20] N. Karnchanachari, M. I. Valls, D. Hoeller, and M. Hutter, "Practical reinforcement learning for mpc: Learning from sparse objectives in under an hour on a real robot," in *Learning for Dynamics and Control*. PMLR, 2020, pp. 211–224.
- [21] K. Chua, R. Calandra, R. McAllister, and S. Levine, "Deep reinforcement learning in a handful of trials using probabilistic dynamics models," *arXiv preprint arXiv:1805.12114*, 2018.
- [22] U. Rosolia and F. Borrelli, "Sample-based learning model predictive control for linear uncertain systems," in *2019 IEEE 58th Conference on Decision and Control (CDC)*. IEEE, 2019, pp. 2702–2707.
- [23] B. Thananjeyan, A. Balakrishna, U. Rosolia, F. Li, R. McAllister, J. E. Gonzalez, S. Levine, F. Borrelli, and K. Goldberg, "Safety augmented value estimation from demonstrations (saved): Safe deep model-based rl for sparse cost robotic tasks," *IEEE Robotics and Automation Letters*, vol. 5, no. 2, pp. 3612–3619, 2020.
- [24] B. Thananjeyan, A. Balakrishna, U. Rosolia, J. E. Gonzalez, A. Ames, and K. Goldberg, "Abc-lmpc: Safe sample-based learning mpc for stochastic nonlinear dynamical systems with adjustable boundary conditions," *arXiv preprint arXiv:2003.01410*, 2020.
- [25] T. P. Lillicrap, J. J. Hunt, A. Pritzel, N. Heess, T. Erez, Y. Tassa, D. Silver, and D. Wierstra, "Continuous control with deep reinforcement learning," *arXiv preprint arXiv:1509.02971*, 2015.
- [26] S. Fujimoto, H. Hoof, and D. Meger, "Addressing function approximation error in actor-critic methods," in *International Conference on Machine Learning*, 2018, pp. 1582–1591.
- [27] S. Levine, A. Kumar, G. Tucker, and J. Fu, "Offline reinforcement learning: Tutorial, review, and perspectives on open problems," *arXiv preprint arXiv:2005.01643*, 2020.
- [28] S. Fujimoto, D. Meger, and D. Precup, "Off-policy deep reinforcement learning without exploration," in *International Conference on Machine Learning*. PMLR, 2019, pp. 2052–2062.
- [29] L.-J. Lin, "Self-improving reactive agents based on reinforcement learning, planning and teaching," *Machine learning*, vol. 8, no. 3-4, pp. 293–321, 1992.
- [30] G. Mahler, A. Winckler, S. A. Fayazi, M. Filusch, and A. Vahidi, "Cellular communication of traffic signal state to connected vehicles for arterial eco-driving," in *2017 IEEE 20th International Conference on Intelligent Transportation Systems (ITSC)*. IEEE, 2017, pp. 1–6.
- [31] P. A. Lopez, M. Behrisch, L. Bieker-Walz, J. Erdmann, Y.-P. Flötteröd, R. Hilbrich, L. Lücken, J. Rummel, P. Wagner, and E. Wießner, "Microscopic traffic simulation using sumo," in *The 21st IEEE International Conference on Intelligent Transportation Systems*. IEEE, 2018. [Online]. Available: <https://elib.dlr.de/124092/>
- [32] OpenStreetMap contributors, "Planet dump retrieved from <https://planet.osm.org>," <https://www.openstreetmap.org>, 2017.
- [33] N. Heess, D. TB, S. Sriram, J. Lemmon, J. Merel, G. Wayne, Y. Tassa, T. Erez, Z. Wang, S. Eslami *et al.*, "Emergence of locomotion behaviours in rich environments," *arXiv preprint arXiv:1707.02286*, 2017.
- [34] F. Borrelli, A. Bemporad, and M. Morari, *Predictive control for linear and hybrid systems*. Cambridge University Press, 2017.
- [35] C. J. C. H. Watkins, "Learning from delayed rewards," 1989.
- [36] Z. Wang, T. Schaul, M. Hessel, H. Hasselt, M. Lanctot, and N. Freitas, "Dueling network architectures for deep reinforcement learning," in *International conference on machine learning*. PMLR, 2016, pp. 1995–2003.
- [37] D. P. Kingma and M. Welling, "Auto-encoding variational bayes," *arXiv preprint arXiv:1312.6114*, 2013.
- [38] D. Silver, G. Lever, N. Heess, T. Degris, D. Wierstra, and M. Riedmiller, "Deterministic policy gradient algorithms," in *International conference on machine learning*. PMLR, 2014, pp. 387–395.
- [39] A. Karpathy, J. Johnson, and L. Fei-Fei, "Visualizing and understanding recurrent networks," *arXiv preprint arXiv:1506.02078*, 2015.
- [40] O. Sundstrom and L. Guzzella, "A generic dynamic programming matlab function," in *2009 IEEE control applications (CCA) & intelligent control (ISIC)*. IEEE, 2009, pp. 1625–1630.
- [41] Z. Zhu, S. Gupta, N. Pivaro, S. R. Deshpande, and M. Canova, "A GPU implementation of a look-ahead optimal controller for eco-driving based on dynamic programming," *arXiv preprint arXiv:2104.01284*, 2021.
- [42] A. Nagabandi, G. Kahn, R. S. Fearing, and S. Levine, "Neural network dynamics for model-based deep reinforcement learning with model-free fine-tuning," in *2018 IEEE International Conference on Robotics and Automation (ICRA)*. IEEE, 2018, pp. 7559–7566.
- [43] A. v. d. Oord, S. Dieleman, H. Zen, K. Simonyan, O. Vinyals, A. Graves, N. Kalchbrenner, A. Senior, and K. Kavukcuoglu, "Wavenet: A generative model for raw audio," *arXiv preprint arXiv:1609.03499*, 2016.
- [44] S. Bai, J. Z. Kolter, and V. Koltun, "An empirical evaluation of generic convolutional and recurrent networks for sequence modeling," *arXiv preprint arXiv:1803.01271*, 2018.
- [45] O. S. Center, "Ohio supercomputer center," 1987. [Online]. Available: <http://osc.edu/ark:/19495/f5s1ph73>
- [46] S. Gupta, S. R. Deshpande, P. Tulpule, M. Canova, and G. Rizzoni, "An enhanced driver model for evaluating fuel economy on real-world routes," *IFAC-PapersOnLine*, vol. 52, no. 5, pp. 574–579, 2019.
- [47] R. J. Williams, "Simple statistical gradient-following algorithms for connectionist reinforcement learning," *Machine learning*, vol. 8, no. 3-4, pp. 229–256, 1992.